Indian Journal of Engineering & Materials Sciences
Vol. 27, June 2020, pp. 538-553

A probabilistic model of acoustic emissions generated during compression test of cementitious materials for crack mode classification

R Vidya Sagar

Department of Civil Engineering, Indian Institute of Science, Bangalore 560 012, India

Received:05 March 2018 ; Accepted:20 November 2019

This article presents a study on crack mode classification in cementitious materials under uniaxial compression using gaussian mixture modeling (GMM) of acoustic emissions approach. To implement a retrofitting method to an *in-service* concrete structure, a prior knowledge about the type of crack developed in the concrete structure is useful. Because, occurrence of AE events during fracture process in solids is random, a probabilsitc method has been required to classify the AE sources related to different types of cracks. In this study, a monotonically increasing unconfined uniaxial compressive load has been applied on different cylindrical specimens of plain cement concrete cast with maximum coarse aggregate size of 20 mm, 12.5 mm and cement mortar to study crack classification. It has been observed that the slope of the line separating the AE data clusters belonging to tensile and shear cracks is more steep for the concrete specimen containing 20 mm maximum coarse aggregate when compared to the concrete specimen containing 12.5 mm maximum coarse aggregate and cement mortar. This indicated that as the coarse aggregate size in concrete increased, the generated AE events related to shear cracking decreased. Also, the AE based *b*-value has reached minimum at the peak load. At the time of failure, AE related to shear cracking has increased sharply.

Keywords: Cementitious materials, Aggregates, Compressive strength, Cracks and cracking, Failure, Mortar, Non-destructive testing, Stress

1 Introduction

Research studies have been focused on global monitoring of large reinforced concrete (RC) structures using acoustic emission (AE) testing[1]. This AE testing is an on-line nondestructive testing (NDT) method and is useful to identify the crack location in the structure or solid which is under stress. Also this passive NDT method is useful to study fracture process only when the crack is moving or in dynamic state. By using this AE testing the entire structure can be monitored at once. AE are the stress waves produced by the sudden internal stress redistribution of the materials caused due to the changes in the internal (micro) structure of the material[2]. A shematic representation of an AE waveform is shown in Fig. 1a. The released AE can be detected using piezoelectric transducers (PZT sensors) mounted on the surface of the test specimen/structure[3-5]. In concrete, the released AE waves during fracture process have frequency range between few kHz to several 100 kHz. During the initial stages of crack formation, the frequency of released AE is high and as the coalescence of micro-cracks to form macro-crack occurs, the frequency reduces to a few kHz[6].In RC structures, columnis most important compression member as it supports the whole structure. Most of the columns, especially short columns are subjected to axial comprerssive load and crack classification of these structural members are important. Hence, the study of fracture of concrete in compression is required.

By using the generated AE, the mode of cracking (tensile or shear) in concrete structures can be studied. Different modes of cracking in concrete structures emit different types of AE waveforms. Researchers attempted to study the location of the cracks and to characterise the source mechanisms such as crack growth, matrix cracking and friction between the two fractured surfaces in concrete structures using AE testing[5,7]. Behnia *et al.* reviewed application of AE testing to concrete structures including available quantitative and qualitative AE methods[8]. Aggelis studied the classification of crack in concrete using AE parameters[9]. One of the earliest studies made to crack classification in concrete structures using AE testing were by JCMS (Japan Construction Material Standards). JCMS recommendations considered two AE wave parameters namely RA and AF as shown in

*Corresponding author (E-mail: rvsagar@iisc.ac.in)

Fig. 1b. The parameter RA [=rise time/peak amplitude] and average frequency (AF)[=counts/duration] are the AE signal parameters used for separating the released AE of tensile and shear cracks into two clusters[10]. Farhidzadeh *et al.* studied crack classification in shear wall tested in laboratory under displacement controlled quasi-static reversed cyclic loading. Using gaussian mixture modelling (GMM) approach, the recorded AE data was analysed and it was concluded that this method was capable of identifying three stages, namely, the dominance of tensile crack stage, the transition stage and the dominance of shear crack stage[11].

Previously, researchers attempted to study the classification of cracking based on the AE parameters namely RA and AF (JCMS-III method). Also the

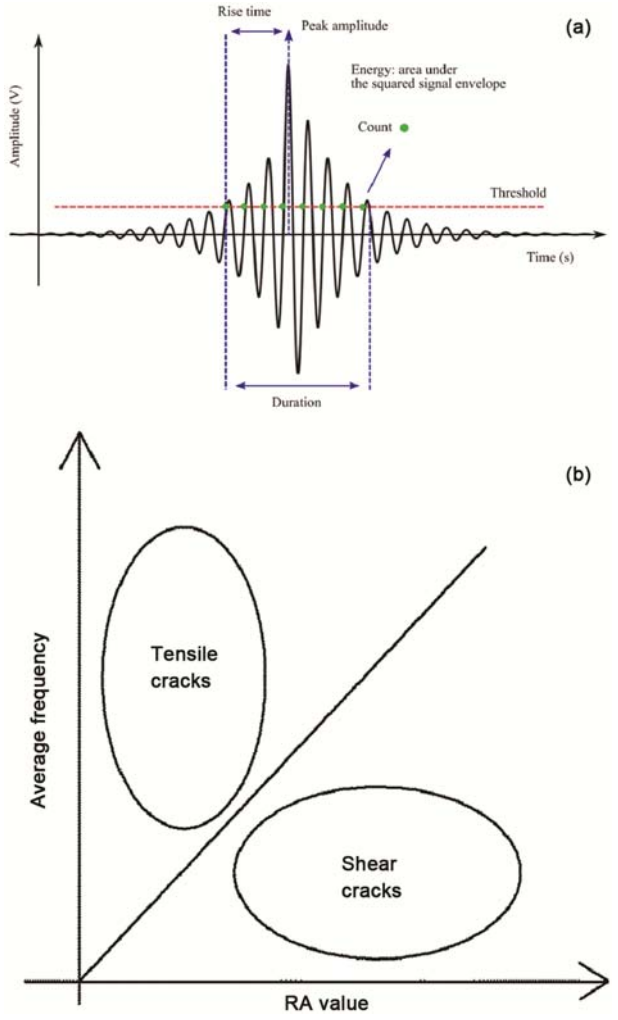

Fig. 1 — (a) A schematic representation of a AE waveform and corresponding parameters and (b) Crack classification in cement concrete as per JCMS-III B5706 code[6].

results were compared with the AE signal based analysis known as Simplyfied Green's functions for moment tensor analysis (SiGMA). It was concluded that these two analyses methods showed similar results and the parameters of the first arrival of AE signal have more important information on crack generation than other AE signals[12,13]. Aggelis *et al.* studied the AE released during the fracture of cementitious materials subjected to four point bending and compared the results with ultrasonic testing. It was concluded that results obtained using AE testing, computed tomography (CT) scan were in good agreement and can be used to study fracture process in concrete[14]. Also, researchers observed that the AF of AE signals shifted to lower level and RA showed rise when micro-cracks coalesce to form macro-cracks in steel fiber reinforced concrete[15,16]. Experimental studies on classification of cracks due to bending of beam by three point bending test and also shear wall subjected to incremental cyclic loads were attempted[8,16]. Wu *et al.* studied the influence of coarse aggregate size on the mechanical properties of concrete under uniaxial compression and three-point bending. It was observed that AE peak amplitude distribution showed a good correlation between the high peak amplitude, AE hits and the growth of the unstable cracks[17]. Further, several attempts have been made to study the fracture process inconcrete to classify the crack mode based on the AE released[18-21]. Saliba *et al.* studied the damage in RC beams under creep using another clustering method known as K-means method[22]. The K-means method is used to obtain an unsupervised classification of multi-dimensional data based on the damage mechanisms[23]. There have been several studies reported on frequency analysis of AE applied to metals and compositematerials[24-28].

However, according to Ohno and Othsu, AE measurement data are random and mostly non linearly separable[12]. Hence, to study crack classification a well defined robust classification algorithm is needed[11]. A probabilistic approach based on GMM is introduced to take into account the random nature of occurrence of AE events for classifying AE sources sources belonging to tensile cracking and shear cracking[11].

The understanding of physical mechanisms that influence the fracture processes in concrete structures and the generated AE has been relatively less[28] because, failure occuring at atomic level in a solid results in acoustic emission. To implement a

retrofitting method to an existing concrete structure *in-service*, a prior knowledge about the type of the crack developed is useful. Based on the type of crack developed due to tensile cracking or shear cracking, engineers can implement the appropriate retrofitting method. Therefore, it is useful to study wheather cracks developed are due to tensile cracking or shear cracking in the existing structure. Hence, a studyfocus on classification of cracks due to uniaxial compression on cementitous material is required.

2 Aim of the Study

It is known that the occurrence of AE events are random in nature. Therefore, a probabilistic analysis of the recorded AE signals to classify the AE belong to tensile crack and shear cracks occurring during compression of concrete and cement mortar specimens subjected to uniaxial compression is used. Further, a study on influence of coarse aggregate on the AE characteristics and crack classification in cementitious materials under compression is attempted.

3 Methodology

The GMM algorithm is a multivariate probabilistic analysis which allows the user to sort large quantity of data into different clusters using the Expectation - Maximization algorithm. In order to classify the data into tensile and shear crack clusters, the GMM method has been used. The GMM or the linear superposition of Gaussians is given in Eq. (1)[29].

$$p(x) = \sum_{k=1}^{K} \pi_k N\left(x \middle| \mu_{k,} \sum \quad _k\right) \quad \ldots(1)$$

where, K is the number of Gaussians and k = 1,… K, $N(x|\mu_{k,}\sum_k)$ is the normal multivariate Gaussian distribution for class K, π_k is the mixing coefficient or the weightage for each Gaussian distribution. A D-variate Gaussian distribution function is given in Eq. (2):

$$N\left(x \middle| \mu_{k,}\sum_k\right) = \frac{1}{(2\pi)^{D/2}\,|\sum|^{1/2}} e^{\frac{-1}{2}[(x-\mu)^T\sum^{-1}(x-\mu)]} \quad \ldots (2)$$

$\mu_k$is the vector form of mean for the k[th] Gaussian, $\sum_k$ is the covariance matrix for the k[th] Gaussian. The mixing coefficient or the weightage, satisfies the constraint 0 $\pi_k \leq 1$ and

$$\sum_{k=1}^{K} \pi_k = 1 \quad \ldots (3)$$

A more details about GMM are given in references Farihdzadeh *et al.*, Reynolds, Ercolino *et al.*, Ramesh[11,30-32].

4 Experimental program

4.1 Materials and Test Specimens

Concrete specimens cast with 20 mm and 12.5 mm of maximum coarse aggregate size and cement mortar were tested under unconfined uniaxial compression. The cylindrical specimens are 300 mm in height and 150 mm in diameter. Ordinary Portland Cement (OPC) of 53 grade (Indian Standard-IS 12269:2013), river sand, coarse aggregates and water were used to prepare the cement concrete specimens. The cement concrete and mortar mixture details are given in Table 1.

4.2. Experimental Setup and AE Instrumentation

The tests were performed using hydraulic load control testing machine. The test setup is shown in Fig. 2a. The load was applied at a rate of 2.5 kN/s[33].During testing for every 15 seconds corresponding load was recorded manually till failure of the specimen. In order to study the AE characterstics during the compressive fracture process of cement concrete and cement mortar, the released AE was recorded. A multi-channel AE monitoring

Table 1 — Cement concrete and mortar mixture proportions (kg/m^3) and compressive strength.

	Cement mortar	Cement Concrete (Maximum size of coarse aggregate is 12.5 mm)	Cement Concrete (Maximum size of coarse aggregate is 20 mm)
Cement	205.3	342.9	343.2
Fine aggregate (4.75 mm)	1580	606.4	606.6
Coarse aggregate (20 mm)	0	0	707.8
Coarse aggregate (12.5 mm)	0	1179.4	471.7
Water content	141.6	182.8	180.8
Water/cement ratio	0.68	0.53	0.53
28-day cylinder compressive strength (MPa)	3.52	44.4	39.9
Tensile strength (MPa)	*****	****	3.21

system which includes six resonant type AE differential sensors, preamplifiers, data acquisition system and processing instrumentation was used. AE^{win} SAMOS and R6D sensors from physical acoustics corporation (PAC), NJ, USA were used. The AE sensor has peak sensitivity at 57 dB with reference to 1 V/(m/s). AE sensors, working in frequency ranges of 35 kHz-100 kHz, were mounted on the surface of the specimen. The response was nearly same for all the resonant differential sensors used in this experimental study. A schematic diagram of a concrete cylindrical specimen mounted with AE sensors is shown in Fig. 2b.The total AE energy released was calculated by summing up the AE energy recorded by 6 channels.AE sensor location coordinates are shown in Table 2. A threshold value of 40 dB was set to filter out environmental background noise. The sampling rate of 1 MSPS was used. A thin layer of silicon grease was used as couplant between AE sensor surface and test specimen.

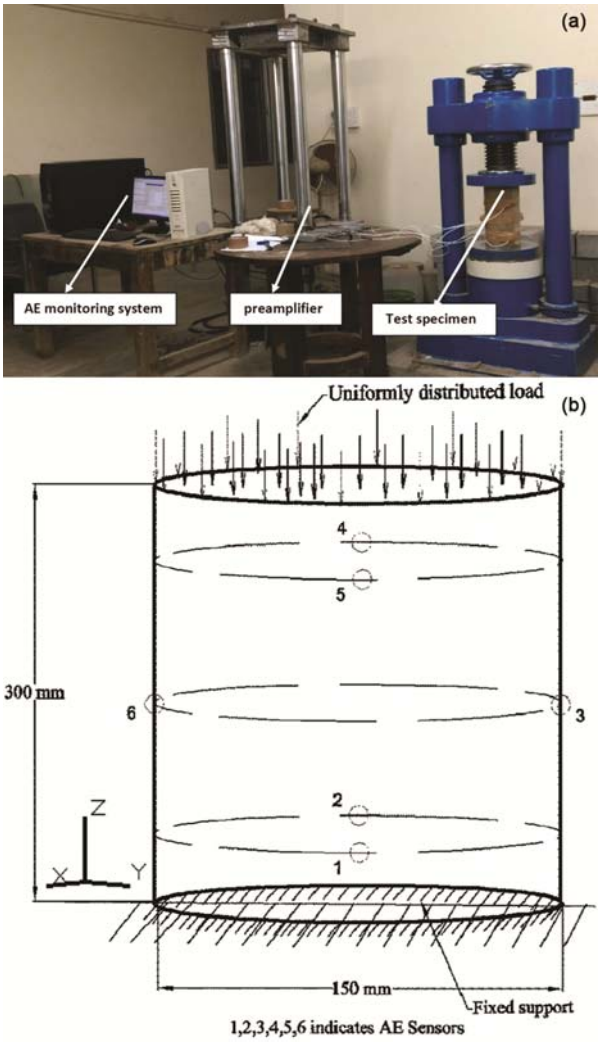

Fig. 2 — (a) Concrete cylinder specimen mounted with AE sensors in the test setup, Structures Laboratory, Department of Civil Engineering, Indian Institute of Science, Bangalore, India and (b) Schematic representation of location of AE sensors mounted on the test specimen.

5 Results and Discussion

5.1 Influence of Coarse Aggregate on AE Characteristics of Cementitious Materials under Uniaxial Compression

Recorded load versus time and load versus hits and energy is shown in Fig. 3. It is observed that the coarse aggregate size has influence on the AE released during the fracture process. In the initial stage, the cumulative AE energy curve shows a concave trend and gradually increased. When the load reaches near to the peak, the cumulative energy showed a sudden rise. This sudden rise could be due to micro-crack formation and simultaneous coalescence of micro-cracks to form macro-cracks resulting in the release of more AE energy. It is observed that the specimen cast with 20 mm coarse aggregate is able to withstand lesser load when compared to the specimen with 12.5 mm coarse aggregate. The reason could be due to the higher aggregate-cement ratio in 20 mm coarse aggregate specimen which reduces the compressive strength of the concrete considerably. Further experimental study is required to confirm the same.

The total cumulative AE energy (volt-s) recorded for the specimen cast with 20 mm maximum coarse

Table 2 — AE Sensor location coordinates.

AE Channel number	AE Sensor location Coordinates (3D Cylinderical)		
	X (mm)	Y (mm)	Z (mm)
1	150	75	75
2	0	75	75
3	75	150	150
4	0	75	225
5	150	75	225
6	75	0	150

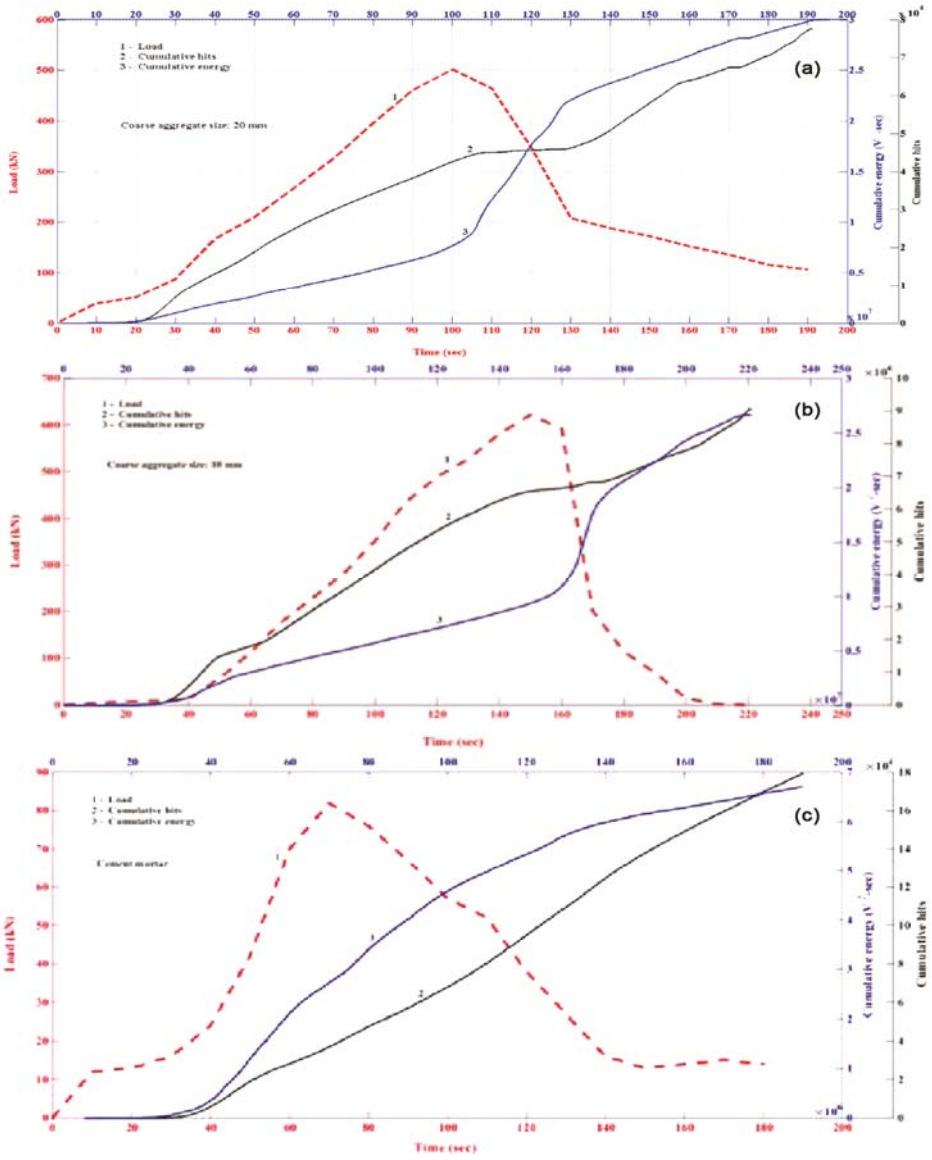

Fig. 3 — A typical recorded plot showing the variation of cumulative hits, energy with load for specimen containing (a) 20 mm maximum coarse aggregate, (b) 10 mm maximum coarse aggregate and (c) Cement mortar [Note: AE energy units are volt-s].

aggregate is lower than the 12.5 mm maximum coarse aggregate specimen as shown in Fig. 4. This may be due to the larger surface area of the 20 mm coarse aggregate. The AE released during the formation of crack, when propagating through the specimen may get attenuated, scattered or absorbed by the 20 mm coarse aggregate. This is further explained in the following sections 5.1.1 and 5.1.2.

5.1.1. AE signal scattering

The AE energy released depends on concrete mixture composition, size of coarse aggregate, strength of the specimen. It is observed that the energy recorded for the specimen containing 20 mm maximum coarse aggregate is less when compared to the energy recorded for the specimen containing 12.5 mm maximum coarse aggregate. The presence of large size aggregates in the specimen cast with 20 mm maximum coarse aggregate results in a scattering effect of the AE signal. The AE wave is forced to deviate from its initial path and this deviation might be the cause for the less energy recorded. The relation between ultrasonic pulse velocity and its frequency are given in Eq. (4).

$$V = f.\lambda \qquad \ldots(4)$$

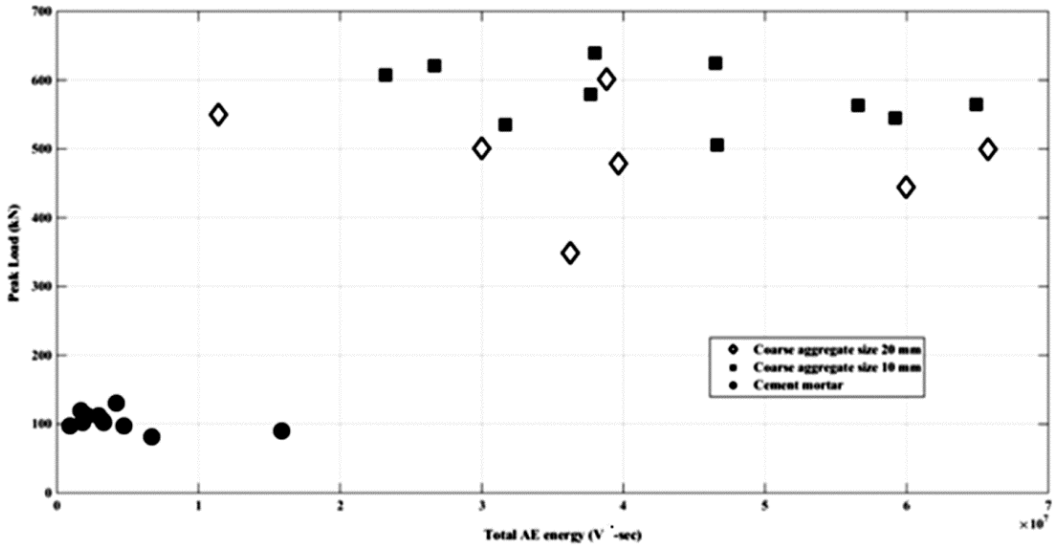

Fig. 4 — Total AE energy (volt-s) recorded.

In Eq. (4),*V* is the velocity of the AE waves, 'λ' is the wavelength and '*f*' is the frequency. For a typical ultrasonic pulse velocity (UPV) of 4000 m/s, using Eq. (4) a frequency of 200 kHz is obtained. This frequency is well within the range of frequencies for AE signal released in concrete, considering a typical AE frequency range for fracture of concrete to lie between 60 kHz and 500 kHz. The corresponding wavelengths using Eq. (4) would be 67 mm - 8 mm, respectively. Since both the cement concrete specimens have coarse aggregate size in this range (i.e. 20 mm and 12.5 mm coarse aggregate), it leads to ultrasonic wave scattering in the specimen. This ultrasonic wave scattering is more in the specimen containing 20 mm maximum coarse aggregate than in the specimen containing 12.5 mm maximum coarse aggregate.

5.1.2. Ultrasonic wave attenuation

Further, the finesse and particles cause the attenuation in the high frequency range beyond 200 kHz. The presence of air bubbles in the specimen results in the attenuation of lower frequency range below 200 kHz, depending on the quantity of fine aggregates present in the concrete mixture[31].The same can be applied in this study, since the frequency is of 200 kHz for specimen containing 20 mm maximum coarse aggregate. The finesse and particles along with the air bubbles may result in ultrasonic sound wave attenuation.

Whereas, in the specimen containing 12.5 mm maximum coarse aggregate the frequency is in the range of 400 kHz. Hence, the signal attenuation may be mainly due to the finesse and particles. This shows that the AE energy recorded for specimen containing 20 mm maximum coarse aggregate [2.5×10^7 V^2-s] is less when compared to specimen containing 12.5 mm maximum coarse aggregate [3.7×10^7 V^2-s].

5.1.3. AE signal absorption

The AE energy loss due to absorption in concrete specimen cast with larger aggregate size is more when compared to specimens with smaller aggregate size and cement mortar[34,35]. The absorption by larger size aggregate might lead to more energy loss and hence the energy recordedis less in the case of specimen containing 20 mm maximum coarse aggregate than the specimen containing12.5 mm maximum coarse aggregate. It was observed that the cement mortar specimens showed less scatter and the specimens containing 20 mm maximum coarse aggregate showed more scatter.

5.2 Classification of Cracks in Cementitious Material under Uniaxial Compression based on Gaussian Mixture Modeling(GMM) of Released AE

In this present study, GMM has been implemented for the analysis of recorded AE data to classify the cracks based on RA and AF into two clusters namely, tensile crack cluster and shear crack cluster. Tensile cracks have higher peak amplitude and hence lower RA (rise time/amplitude) and shear cracks have lower amplitude and hence higher RA. The data in the tension cluster has been denoted as '+' and the shear cluster by 'o'. Two time intervals before the peak load are t_1, t_2 and two time intervals after the peak load aret_3, t_4 until failure have been considered as shown in Fig. 5 and the time interval values are given in Table 3.

For the specimen containing maximum aggregate size of 20 mm, the tensile cracks occur predominantly during the initial stages before reaching the peak load. This indicates that there is excessive micro-cracks occurring in the specimen as shown in Fig. 6a and Fig. 6b. For the time interval t_3, it is observed that there is a transition from the tensile crack cluster to the shear crack cluster indicating that micro cracks are coalescing to form macro-cracks as shown in Fig. 6c. Later, for the time interval t_4, until the failure of the specimen, there is significant increase in the shear cracks upon further loading with very less tensile crack formation as shown in Fig. 6d. In the contour plots shown in Fig. 6(a–d), for the different time intervals t_1, t_2, t_3 and t_4, it is observed that the number of tension cracks and shear cracks vary and hence the shape of the contour changes. The probability density (denoted by the secondary y-axis) related to the occurrence of tension cracks and shear cracks as shown in the contour plot, also varies for the specimen containing 20 mm maximum coarse aggregate.

Variation of load with time and time intervals considered for concrete cast with 12.5 mm coarse aggregates is shown in Fig. 7. It is observed that in case of specimen containing 12.5 mm maximum coarse aggregate that, the shear cracks also occur in considerable proportion in the time interval $t_2$just before reaching the pre-peak load as shown in Fig. 8b.Variation of load with time related to compression test of cement mortar is shown in Fig. 9. In the same figure t_1, t_2, t_3 and t_4 denotes the time intervals considered for crack mode classifcation using AE testing. It is observed that the tensile cracks and shear cracks occur from the initial loading stage t_1 until the failure t_4 as shown in Fig. 10(a–d) in case of cement mortar. In all the three different specimens, the ultimate failure occurs due to excessive shear crack and coalescence of micro-cracks to form macro-cracks. The posterior probability which represents the formation of tension cracks and shear cracks (secondary y-axis of the scatter plot) is varying. This variation in posterior probability and probability

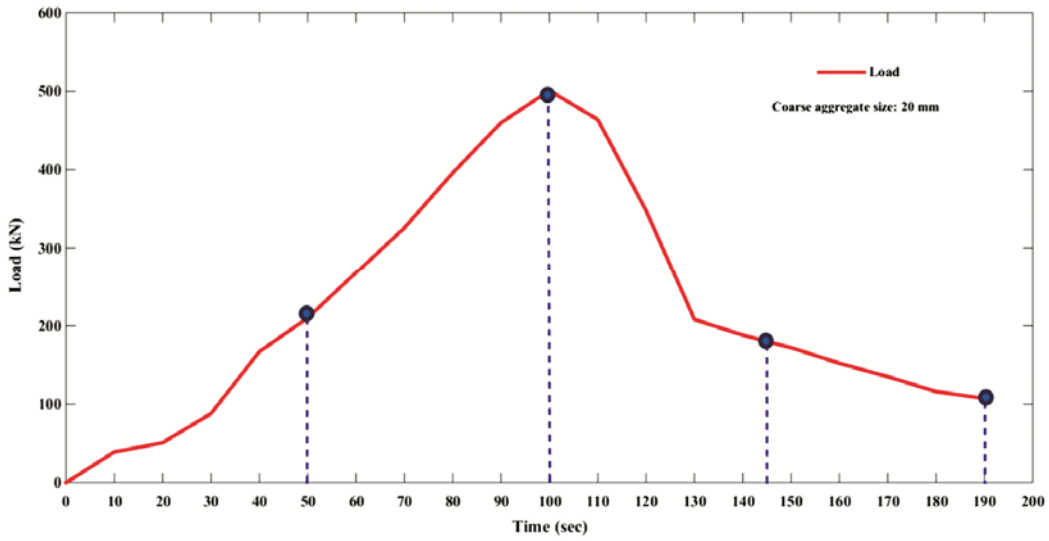

Fig. 5 — Variation of load with time. t_1, t_2, t_3 and t_4 denotes the time internal for crack mode classifcation using Gaussian mixture modeling (concrete cast with 20 mm maximum coarse aggregate).

Table 3 — Time intervals considered for crack classification using GMM algorithm

Interval	Concrete (aggregate size 20 mm)		Concrete (aggregate size12.5 mm)		Cement mortar	
	Initial time (s)	Final time (s)	Initial time (s)	Final time (s)	Initial time (s)	Final time (s)
I	0	50	0	80	0	40
II	50	100	80	150	40	70
III	100	145	150	180	70	120
IV	145	190	180	220	120	180

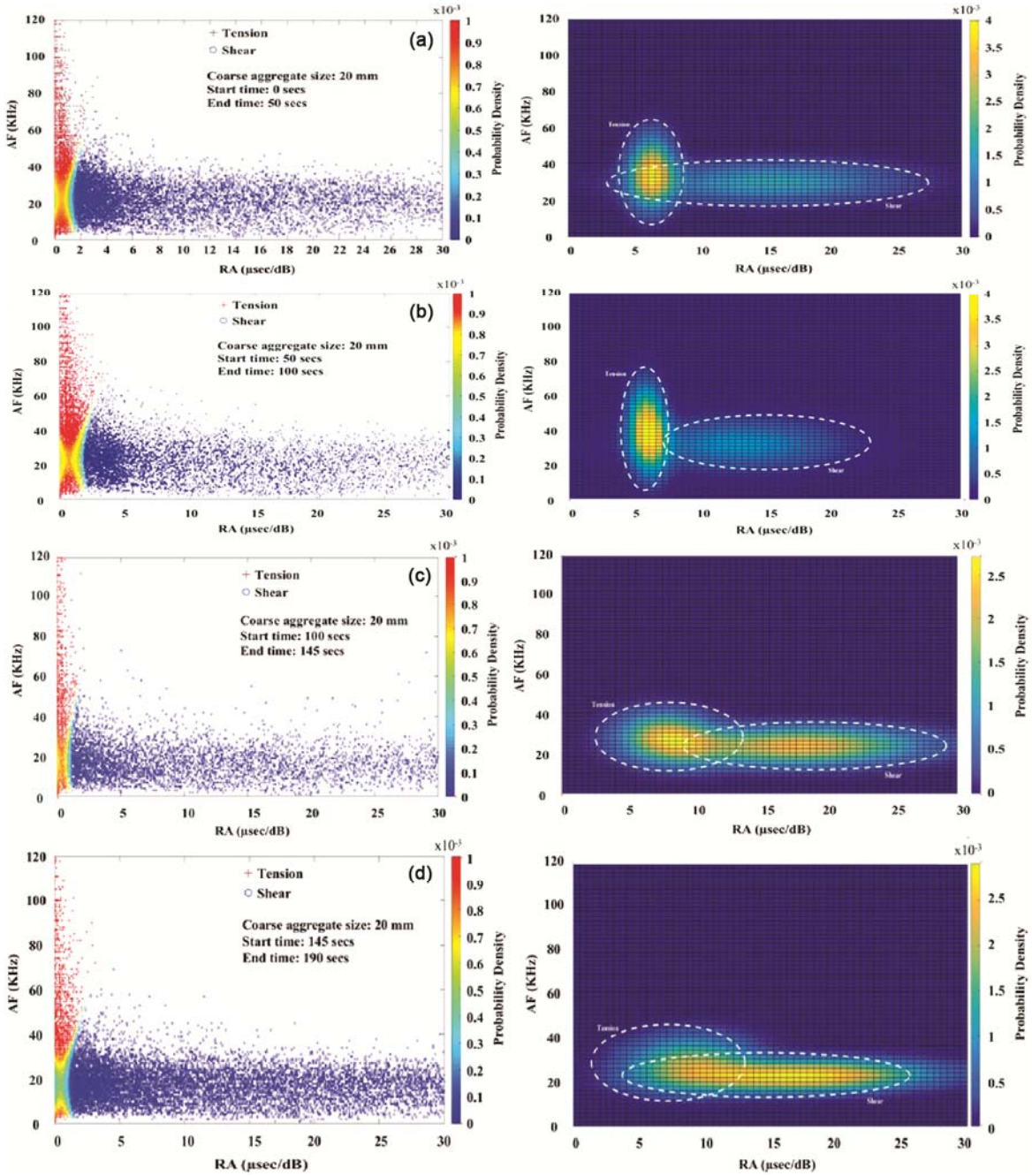

Fig. 6 — Gaussian mixture modeling plots for different time intervals (concrete cast with maximum coarse aggregate size of 20 mm).

density for the specimen cement mortar, concrete containing 12.5 mm maximum coarse aggregate and 20 mm are shown in Fig. 11(a–c), respectively.

5.3 Method to Separate AE clusters related to Tensile and Shear Cracks

The separator line intersecting the *x*-axis (RA value) for the three different cementitious specimens is obtained by drawing a perpendicular bisector (shown by dash-dot line in Fig. 11(a –c) to the line joining the mean of the clusters. It is observed that in the case of cement mortar specimen the separator line intersects the *x*-axis (RA value) at 5 μs/dB. However in case of specimens containing 12.5 mm maximum size coarse aggregate, the separator line intersects at 15 μs/dB. For the specimen containing 20 mm maximum size coarse aggregate, it intersects at RA value of 21 μs/dB.

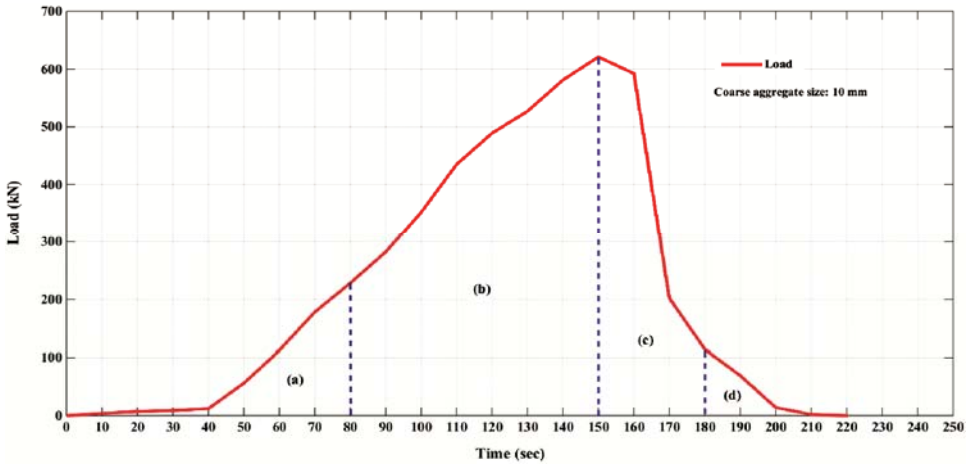

Fig. 7 — Variation of load with time t_1, t_2,t_3 and t_4 denotes the time internal for crack mode classifcation using Gaussian mixture modeling (concrete cast with 12.5 mm maximum size coarse aggregate).

This indicates that there are more tensile cracks than shear cracks occurring in the specimen containing maximum coarse aggregate size of 20 mm. As the coarse aggregate size increases, from fine aggregates in cement mortar to 20 mm coarse aggregate, the tensile cracks increase and the shear cracks reduce. This could be the result of large coarse aggregates resisting the growth of tensile micro-cracks to form shear cracks. Hence, there is a shift in the trend in which the separator line divides the two clusters. It can also be inferred that the coalescence of micro-cracks to form macro-cracks takes place readily in cement mortar specimens when compared to the other two specimens.

Under uniaxial compression shear stresses also develop. Also, it is observed that, under uniaxial compression, the cracks are approximately parallel to the applied load but some cracks form at an angle to the applied load. The parallel cracks are caused by a localized tensile stress in a direction normal to the compressive load; the inclined cracks occur due to the collapse caused by the development of shear planes[36]. Compression test imposes a more complex system of stress, mainly because of lateral forces developed between the end surfaces of the concrete specimen and the adjacent steel platens of the testing machine. These forces are induced by the restraint of the concrete, which attempts to expand laterally (Poisson effect). The effect of platen restraint can be seen from typical failure modes. The effect of shear is always present but its dominance depends upon height to width ratio of specimen. Concrete cylinder unider uniaxial compression fails in three modes, splitting; shear (cone); splitting and shear[33,36].

5.4 Variation of AE based *b*-value and Damage Parameter (D) of Cementitious Material under Compression

The AE based *b*-value is computed using the Gutenberg - Richter empirical relation given in Eq. (5).

$$\log_{10} N(A) = a - b\left(\frac{A_{dB}}{20}\right) \quad \ldots(5)$$

In Eq. (5), A_{dB} is the peak amplitude of the AE (hits or events) in decibels. b is the AE based *b*-value. $N(A)$ is the number of AE hits of amplitude greater than A. '*a*' is a constant determined largely by the background noise present in the surroundings of testing in a laboratory or *in-situ*. '*b*' is the log-linear slope of the frequency of occurence-peak amplitude distribution of AE[37].

It is observed that, a high *b*-value at the start occurs due to release of large number of AE hits indicating nucleation of micro-cracks. A low *b*-value indicates coalescence of micro-cracks to form macro-cracks, releasing energy with high AE amplitude. In this study, similar results are observed for specimen containing 20 mm maximum coarse aggregate as shown in Fig. 12. During the initial stage of loading up to peak load, the *b*-value ranged from 0.6 to 1.5, intermediate *b*-value reduced to 0.1 and as the load was increased, the *b*-value was raised to 1.2 until failure due to strain softening nature of the cementitious material.

In case of cement mortar specimen, the *b*-value ranges from 0.6 to 1.2 initially and at the failure stage it reached a maximum value of 1.6. The cement mortar failed quickly when compared to concrete specimens, hence the *b*-value reached minimum very early.

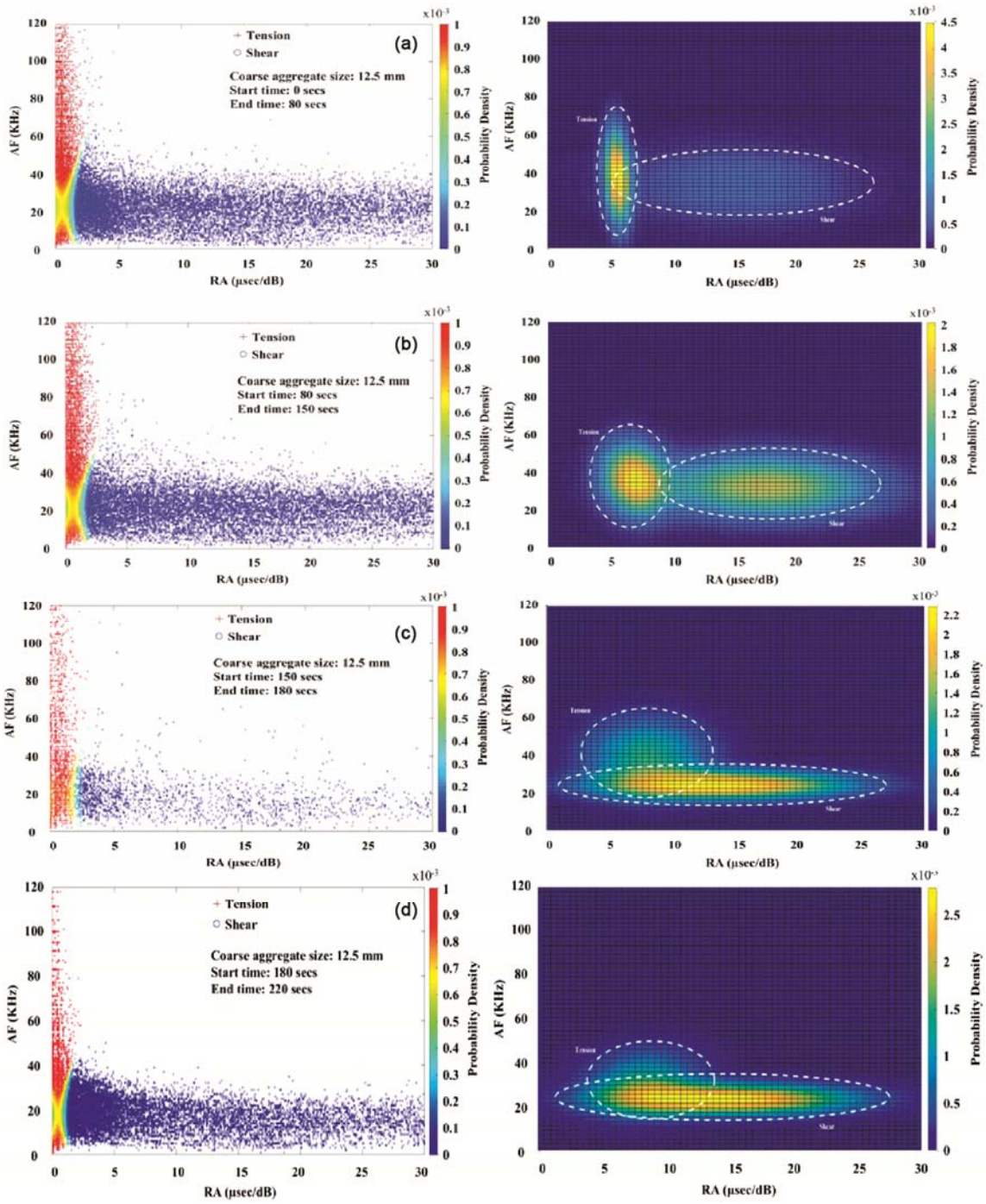

Fig. 8 — Gaussian mixture modeling plots for different time intervals. (concrete cast with coarse aggregate size 12.5 mm).

The difference in the *b*-values indicate that the micro cracks formation is predominant in the initial loading stage for the specimen containing 12.5 mm and 20 mm maximum coarse aggregate size when compared to cement mortar specimen. In all the three specimens, it was observed that in the initial and final loading stages the *b*-value variation is dense and for the peak load time interval, the *b*-value becomes sparse. This indicates that the micro-crack formation in the initial and final stage of loading is large and in the peak load time interval, there is large number of micro-cracks coalescing to form macro-cracks.

Further, the *b*-value is compared with the damage parameter (D) which is used to evaluate the damage in

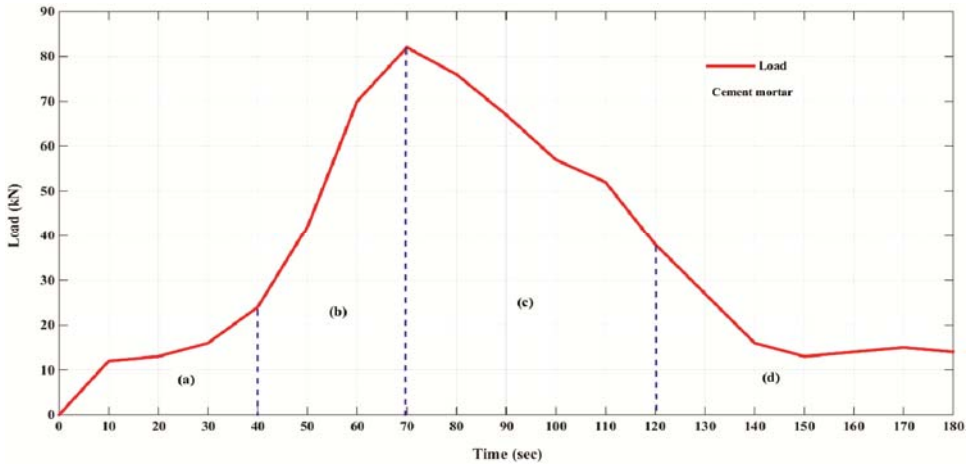

Fig. 9 —Variation of load with time related to compression test of cement mortar. t_1, t_2, t_3 and t_4 denotes the time interval for crack mode classifcation using AE testing.

a material in the context of acoustic emission testing[38]. Damage parameter is proportional to cube of the mean of the crack length and is given in Eq. (6)

$$D = \sum 10^{3.\left(\frac{A_{dB}}{20}\right)} \quad ...(6)$$

Where A_{dB} is the peak amplitude of AE signal in decibels. Both the *b*-value and the damage parameter are calculated for the recorded AE data channel wise and for a group of 100 hits. The damage parameter is normalized with a value of 1.0 representing maximum damage occurring in the specimen. It is observed from Fig. 13(a –c) that when the *b*-value reaches minimum, the damage parameter is maximum. This indicates that the damage in the specimen is maximum and it fails, which is confirmed by the macro-crack widening observed during the testing.

5.5 Relationship between AE based *b*-value and Gaussian Mixture Modeling of AE Results

The total number of AE hits in each cluster is obtained from the GMM for each specimen and is shown in Fig. 14(a –c). The load versus time graph for each specimen has been divided into several time intervals as shown in Table 4 in order to observe the trend in tensile crack and shear crack formation. For all the three specimens, the changing trend has been divided into four phases. It is observed that, in phase-I when the load is gradually applied on the specimen, the tensile crack formation dominates shear crack formation. As the load is increased further, a transition phase (phase-II) is observed where in the tensile cracks reduce and the shear cracks gradually increased. This transition occurs in the time interval comprising the peak load or just after the peak load. Further, in phase-III, it is observed that the shear crack formation suddenly rises indicating that the specimen undergoes yield under increasing load. In the cement mortar specimen the transition phase (phase-II) and the shear crack dominant phase (phase-III) coincide, as the specimen has very less resistance to the compressive load and fails quickly. Hence, a clear transition phase could not be separated from the yielding phase. Further as the load is increased, in phase-IV, the shear cracks rise suddenly leading to the ultimate failure of the specimen.

An attempt has been made to relate the AE based *b*-value and the plot showing AE hits categorized as tension and shear cracks at different time intervals obtained from GMM as shown in Fig. 14(a –c). It is observed that, the time at which the *b*-value reaches a minimum, lies in the time interval corresponding to the yielding of the specimen. From Table 4, the *b*-value reaches a minimum in the time interval TI-5, TI-6 and TI-7 for cement mortar, specimen containing 12.5 mm and specimen containing 20 mm maximum coarse aggregate respectively. It is observed that this time interval corresponds to the phase-III or the phase in which the specimen yields.

6 Practical Significance

It is known that in RC structures, short columns subjected to compressive stress. Also, sometimes, changes in the coarse aggregates size takes place in the concrete due to *in-situ* conditions and practical situations. Therefore, it is required to study the fracture process of concrete in compression.

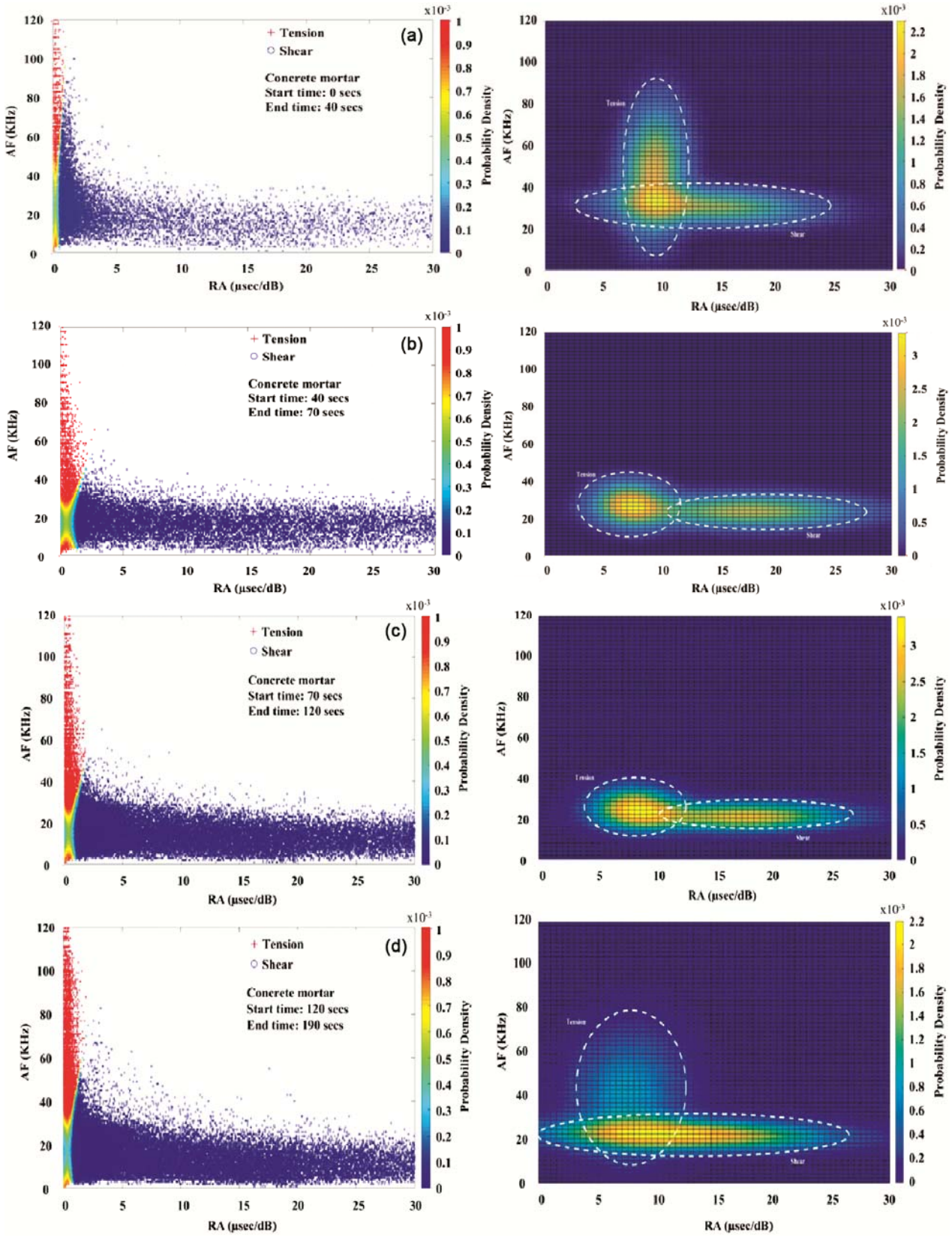

Fig. 10 — Gaussian mixture modeling plots for different time intervals (cement mortar).

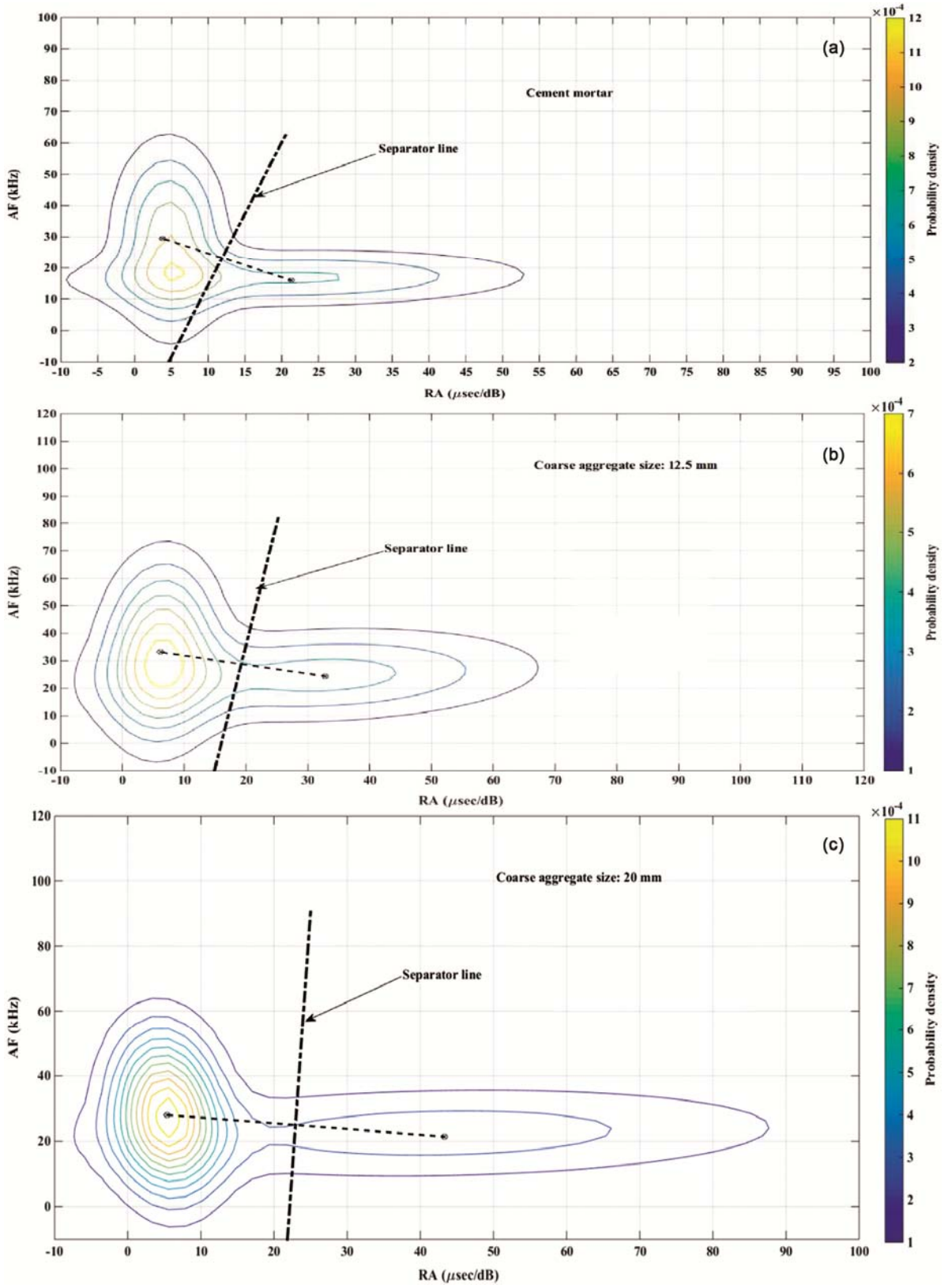

Fig. 11 — Gaussian mixture modeling plot showing separator line dividing the contour into tension and shear crack contour for (a) cement mortar, (b) concrete with 12.5 mm maximum coarse aggregate and (c) concrete with 20 mm maximum coarse aggregate.

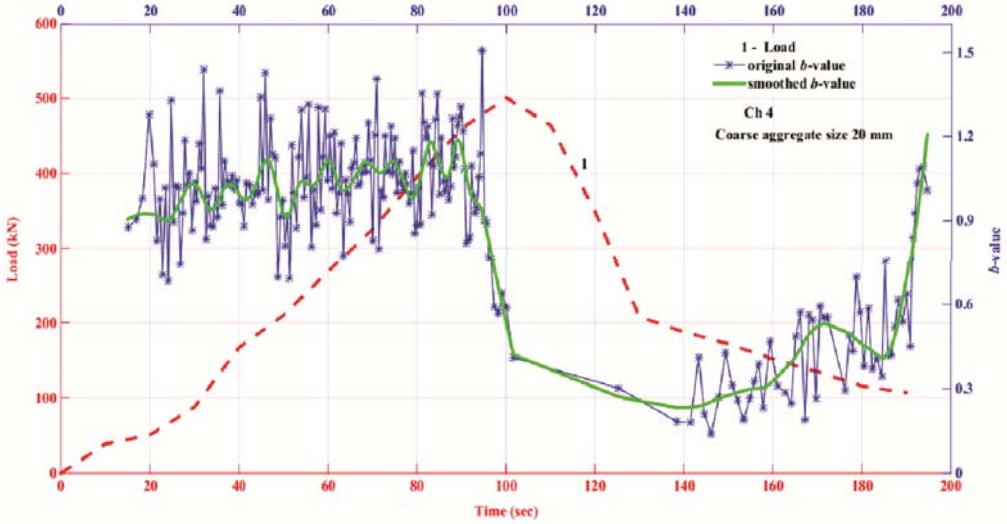

Fig. 12 — AE based *b*- value variation with applied external compressive force for concrete cast with 20 mm aggregate.

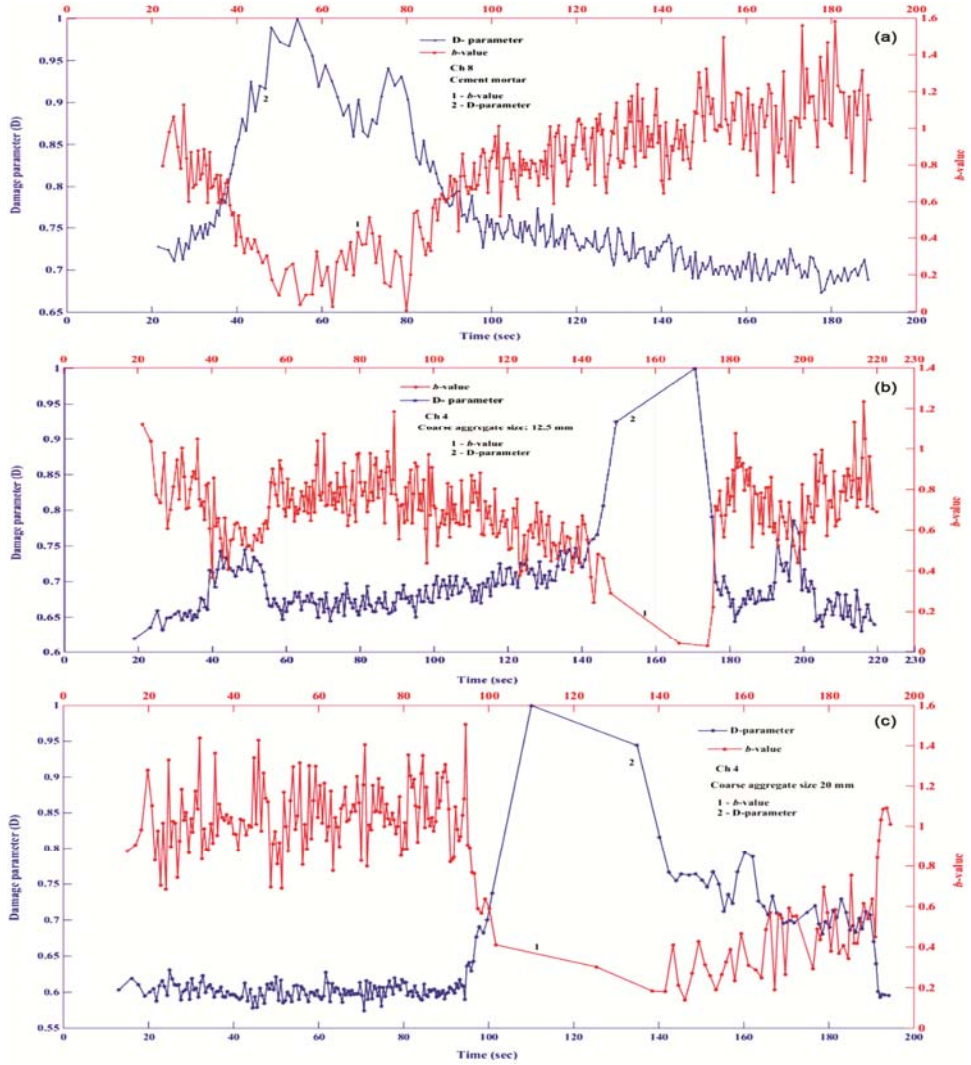

Fig. 13 — Variation of AE based *b*-value and damage parameter (D) (a) cement mortar, (b) specimen containing 12.5 mm maximum coarse aggregate and (c) specimen containing 20 mm maximum coarse aggregate.

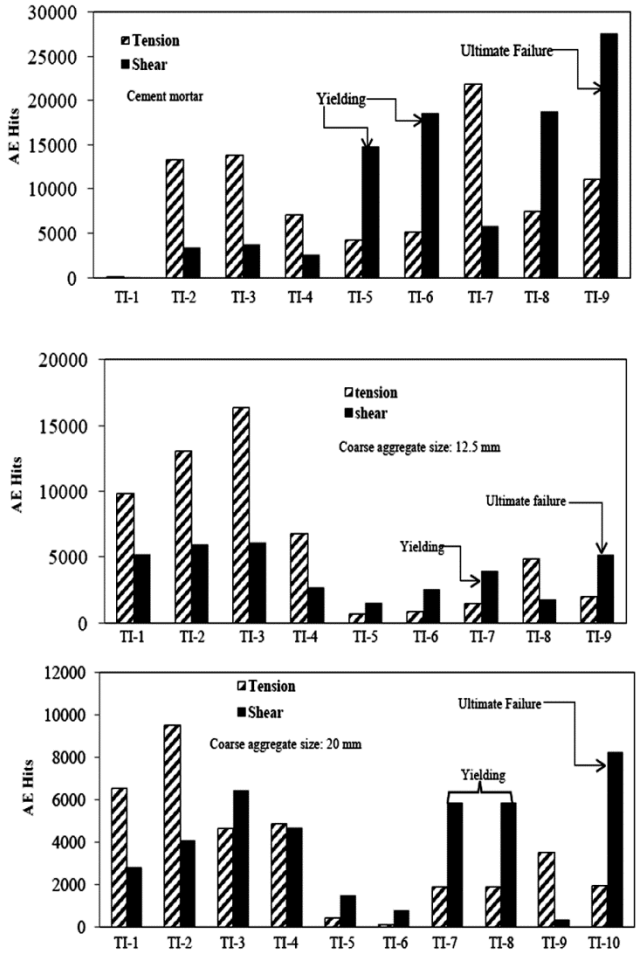

Fig. 14 — Number of AE hits for tensile or shear cracks in the time interval for (a) cement mortar, (b) specimen containing 12.5 mm maximum coarse aggregate and (c) specimen containing 20 mm maximum coarse aggregate.

7 Conclusions

Based on the above experimental study, the given below major conclusions can be drawn.

(i) There is an increase in attenuation, scattering and absorption of AE signals as the coarse aggregate size increases in cementitious.

(ii) By using GMM method, three stages of crack mode were observed, i.e., initial stage where tensile cracks dominate, transition stage between tensile cracks and shear cracks and the final stage where shear cracks dominate.

(iii) The separator line changed to more steep for specimen containing maximum coarse aggregate size of 20 mm. This indicates that as the coarse aggregate size increases, less percentage of AE events during shear cracks are recorded.

(iv) For the three different cementitious materials, the time at which the AE based *b*-value reaches minimum corresponds to the time when there is sudden rise in shear cracks following the transition phase as seen from the GMM of AE analysis plots. At the same instant, it is observed that the specimen yielded.

(v) When the *b*-value decreases, the damage parameter (D) increases indicating that when the *b*-value is low there is maximum damage taking place in the specimen (i.e. more number of micro cracks coalesce to form macro cracks and subsequent crack growth) and is observed to take place near to the peak load.

(vi) The amount of finesse and particles and higher air bubbles present in the specimen containing

Table 4 —Time interval chosen to show the point at which the specimen is yielding and the corresponding *b*- value range (values in bold indicates the specimen is undergoing yielding).

Time interval	Cement mortar				Cement Concrete (Maximum coarse aggregate size: 12.5 mm)				Cement Concrete (Maximum coarse aggregate size: 20 mm)			
	Time (s)		*b*-value range		Time (s)		*b*-value range		Time (s)		*b*-value range	
	T_i	T_j	*b*-value (T_i)	*b*-value (T_j)	T_i	T_j	*b*-value (T_i)	*b*-value (T_j)	T_i	T_j	*b*-value (T_i)	*b*-value (T_j)
TI-1	0	20	-	-	0	40	-	0.7	0	25	-	0.9
TI-2	20	40	0.8	0.5	40	80	0.7	0.75	25	50	0.9	1.0
TI-3	40	60	0.5	0.15	80	120	0.75	0.6	50	75	1.0	1.1
TI-4	60	70	0.15	0.55	120	150	0.6	0.3	75	100	1.1	0.4
TI-5	**70**	**90**	**0.55**	**0.6**	150	165	0.3	0.02	100	115	0.4	0.3
TI-6	90	110	0.6	0.8	**165**	**180**	**0.02**	**0.8**	115	130	0.3	0.25
TI-7	110	130	0.8	1.0	180	195	0.8	0.6	**130**	**145**	**0.25**	**0.3**
TI-8	130	150	1.0	1.1	195	210	0.6	0.8	145	160	0.3	0.35
TI-9	150	180	1.1	1.2	210	220	0.8	0.75	160	175	0.35	0.5
TI-10	-	-	-	-	-	-	-	-	175	190	0.5	0.7

20 mm maximum coarse aggregate causes the attenuation of AE signals. Whereas, the finesse and particles alone result in the attenuation in cement mortar specimen. However, in case of concrete cast with 12.5 mm more coarse aggregates are present in number. This results in lower AE energy being recorded for the 20 mm maximum coarse aggregate specimen than the specimen containing 12.5 mm maximum coarse aggregate. Further experimental study is required to confirm the same.

References

1 Shiotani T, Aggelis D G & Makishima O, *J Bridge Eng*, 14 (2009) 188.
2 Gross C U & Ohtsu M, *Acoustic Emission Testing,* (Springer Heidelberg) 2008, ISBN: 978-3-540-69895-1.
3 RILEM TC 212-ACDi. RILEM *Mat and Str*, 43 (2010) 1177.
4 RILEM TC 212-ACDii. RILEM *Mat and Str*, 43 (2010) 1183.
5 RILEM TC 212-ACDiii. RILEM *Mat and Str*, 43 (2010) 1187.
6 Schiavi A, Niccolini G, Tarizzo P, Carpinteri A, Lacidogna G & Manuello A, *Strain*, 47 (2011) 105.
7 Goszczynska B, Swit G, Trampczynski W, Krampikowska A, Tworzewska J & Tworzewski P, *Arch Civ Mech Eng*, 12 (2012) 23.
8 Behnia A, Chai H K & Shiotani T, *Construc Build Mater*, 65 (2014) 282.
9 Aggelis D G, *Mech Res Comm*, 38 (2011) 153.
10 JCMS – IIIB5706. *Monitoring Method for Active Crack in Concrete by Acoustic emission. Federation of Construction Materials in Industry*, Japan. (2013) 23.
11 Farhidzadeh A, Salamone S & Singla P, *J Intel Mater Sys Struct*, 24 (2013) 1722.
12 Ohno K & Ohtsu M, *Construc Build Mater*, 24 (2010) 2339.
13 Ohtsu M, Okamoto T & Yuyama S, *ACI Struct J*, 95 (1998) 87.
14 Aggellis D G, Shiotani T, Momoki S & Hirama A, *ACI Mater J*, 106 (2009) 509.
15 Aggelis D G, Soulioti D V & Sapouridism N, *Construc Build Mater*, 25 (2011) 126.
16 Farhidzadeh A, Mpalaskas A C, Matikas T E, Farhidzadeh H & Aggelis D G, *Construc Build Mater*, 67 (2014) 129.
17 Wu K, Chen B & Yao W, *Cem Conc Res*, 31 (2001) 919.
18 Aggelis D G, Kordatos E Z, Strantza M, Soulioti D V & Matikas T E, *Construc Build Mater*, 25 (2011) 3089.
19 Aldahdooh M A A & Bunnori N M, *Construc Build Mater*, 45 (2013) 282.
20 Aldahdooh M A A, Bunnori N M & Johari M M, *Construc Build Mater*, 44 (2013) 812.
21 Bunnori N M, Lark R J & Holford K M, *Mag Conc Res*, 63 (2011) 683.
22 Saliba J, Loukili A, Grondin F & Regoin J P, *Mat Str,* 47 (2014) 1041.
23 Ercolino M, Farhidzadeh A, Salamone S & Magliulo G, *Str Health Monit Main*, 2 (2015) 339.
24 Lu C, Ding P & Chen Z, *Proc Eng,* 23 (2011) 210.
25 Marinescu I & Axinte D, *Int J Mach Tools Manuf,* 49 (2009) 53.
26 Ding Y, Reuben R L & Steel J A, *NDTE Int,* 37 (2004) 279.
27 Bayray M & Rauscher F, *Window Fourier transform and wavelet transform in acoustic emission signal analysis*, 25th European Conference on Acoustic Emission Testing, (2002) 37.
28 Qi G & Barhorst A, *Comp Sci Tech*, 57 (1997) 389.
29 Rossi P, Ulm F J & Hachi F, *J Eng Mech*, 122 (1996) 1038.
30 Reynolds D A, *Gaussian Mixture Models*, *Encyclopedia of Biometric Recognition*, (Springer publishers), (2009) 659.
31 Ercolino M, Farhidzadeh A, Salamone S & Magliulo G, *Str Health Monit Main*, 2 (2015) 339.
32 Ramesh S, *Gaussian mixture models and the EM algorithm. MIT-CSAIL*, (MIT, Cambridge, Massachusetts, USA) 2012.
33 ASTM: C 39/C 39M – 03: Standard Test Method for Compressive Strength of Cylindrical Concrete Specimen. ASTM Subcommittee C09.61 on Testing Concrete for Strength. Published October 2003.
34 Landis E N & Baillon L, *J Eng Mech*, 128 (2002) 698.
35 Aggelis D G, Polyzos D & Philippidis T P, *J Mech Phys Solids,* 53 (2005) 857.
36 Neville A A, & Brooks J J, *Concrete technology* (Pearson education publishers) 2006, ISBN: 978-93-534-3655-1.
37 Colombo S, Main I G & Forde M C, *J Mater Civ Eng*, 15 (2003) 280.
38 Cox S J D & Meredith P G, *Int J Rock Mech Mining Sci Geomech Abs,* 30 (1993) 11.